Anomalous dynamical line shapes in a quantum magnet at finite temperature

D. A. Tennant,[1,2] B. Lake,[1,2] A. J. A. James,[3] F. H. L. Essler,[4] S. Notbohm,[1,5] H.-J. Mikeska,[6] J. Fielden,[7] P. Kögerler,[7] P. C. Canfield,[7] and M. T. F. Telling[8]

[1]*Helmholtz-Zentrum Berlin für Materialien und Energie, Hahn-Meitner Platz 1, 14109 Berlin, Germany*
[2]*Institut für Festkörperphysik, Technische Universität Berlin, Hardenbergstrasse 36, D-10623 Berlin, Germany*
[3]*Department of Condensed Matter Physics and Material Science, Brookhaven National Laboratory, Upton, New York 11973-5000, USA*
[4]*Rudolf Peierls Centre for Theoretical Physics, 1 Keble Road, Oxford OX1 3NP, United Kingdom*
[5]*School of Physics and Astronomy, North Haugh, St. Andrews, KY15 9SS, United Kingdom*
[6]*Department of Theoretical Physics, University of Hannover, D-30167 Hannover, Germany*
[7]*Ames Laboratory, Iowa State University, Ames, Iowa 50011, USA*
[8]*ISIS Facility, Rutherford Appleton Laboratory, Chilton, Didcot OX11 OQX, United Kingdom*

(Received 20 November 2011; published 4 January 2012)

The effect of thermal fluctuations on the dynamics of a gapped quantum magnet is studied using inelastic neutron scattering on copper nitrate, a model material for the spin-1/2, one-dimensional (1D) bond alternating Heisenberg chain. A large, highly deuterated, single-crystal sample of copper nitrate is produced using a solution growth method and measurements are made using the high-resolution backscattering spectrometer OSIRIS at the ISIS Facility. Theoretical calculations and numerical analysis are combined to interpret the physical origin of the thermal effects observed in the magnetic spectra. The primary observations are (1) a thermally induced central peak due to intraband scattering, which is similar to Villain scattering familiar from soliton systems in 1D, and (2) the one-magnon quasiparticle pole is seen to develop with temperature into an asymmetric continuum of scattering. We relate this asymmetric line broadening to a thermal strongly correlated state caused by hard-core constraints and quasiparticle interactions. These findings are a counter example to recent assertions of the universality of line broadening in 1D systems and are applicable to a broad range of quantum systems.

DOI: 10.1103/PhysRevB.85.014402 PACS number(s): 75.10.Pq, 75.40.Gb, 75.50.Ee

I. INTRODUCTION

The behavior of quantum systems at finite temperature is of great importance for real applications as well as fundamental science. In spite of this, relatively few experimental studies have been undertaken on quantum magnets. The standard paradigm for temperature effects in a quantum system is lifetime damping of the quasiparticles. This manifests as a Lorentzian-type energy[1–3] or wave vector (phase coherence) broadening.[4] Indeed, for one-dimensional systems, it has been proposed that these linewidths display universality.[5,6] To test the applicability of these ideas more widely, we study a generic one-dimensional system of quasiparticles subject to hard-core interactions (i.e., where more than one quasiparticle cannot simultaneously occupy a site) in the form of the gapped quantum magnet, $Cu(NO_3)_2{\cdot}2.5(D_2O)$ (copper nitrate), by use of inelastic neutron scattering. The advantage of such a system for finite-temperature studies is that while being flexible enough to be a useful description of many real condensed-matter systems, it has a relatively simple excitation spectrum: energy bands are arranged according to the number of quasiparticles, separated by the energy required to create an extra quasiparticle, and can be studied in relative isolation providing that the bandwidth is small. At low temperatures, compared to the band separation, we can then explore the thermal development of scattering from individual quasiparticle modes. Hence, in the following, we can unambiguously identify different aspects of the interplay of quantum and thermal fluctuations.

Our most important finding is the development with increasing temperature of an *asymmetric continuum of scattering* about the single-particle mode that differs strongly from the Lorentzian broadening familiar from conventional theories of thermal effects in magnets, a phenomenon that occurs even though the lifetime broadening is an order of magnitude smaller than the mode frequency. We propose this behavior to be non-system-specific and applicable to a broad range of low-dimensional systems with thermally activated strong correlations. This asymmetric broadening has been missed in previous work[4,6] and shows the limitations on the parameter regime in which universal behavior may emerge. Notwithstanding the former remark, a more recent approach[7,8] does predict asymmetric line broadening for one-dimensional systems described by gapped continuum integrable field theories. The application of this approach to systems that are not exactly solvable[9,10] also predicts an asymmetric broadening. It is then vital to see the degree to which these theoretical predictions match the experimental situation. Accordingly, we take the theory, suitably adapted to the specific case of copper nitrate, and compare it to the inelastic neutron-scattering results, finding qualitative and *quantitative* agreement for temperatures smaller than the gap. The theory takes the form of an expansion in particle number, or, equivalently, temperature, and is therefore not expected to be applicable at higher temperatures. Therefore, we also compare to exact diagonalization results, which, though limited to small system sizes, are not restricted to low temperatures in the same fashion.

Furthermore, such systems will also display *intraband* scattering at finite temperatures when there is a thermally induced population of quasiparticles. Both the experiment and theory described here are capable of accessing the resulting low-frequency response, and we take advantage of this situation to perform an additional test of their agreement.

Probing the aforementioned system of hard-core quasiparticles with neutrons requires it to be manifested as some form of spin system. The alternating Heisenberg chain (AHC) of spin-1/2 moments with strong alternation constitutes such a system. The AHC is described by the Hamiltonian $H = \sum_i J\mathbf{S}_{i,1} \cdot \mathbf{S}_{i,2} + J'\mathbf{S}_{i,2} \cdot \mathbf{S}_{i+1,1}$, where J and J' are antiferromagnetic exchange constants, with $J > J'$ and alternation parameter α defined as J'/J (here, strong alternation corresponds to small α). The AHC has been an important paradigm in quantum magnetism for a long time.[11–13] Recently, it has attracted the attention of the quantum information community as an example for detecting and quantifying entanglement in solids,[14] as well as encoding and transporting qubits.[15]

In the AHC, the dominant antiferromagnetic exchange interaction (J) between two neighboring sites (separated by distance ρ and with chain repeat distance d) couples the spins into pairs, or "dimers," whose ground state is a singlet $1/\sqrt{2}\{|\uparrow\downarrow\rangle - |\downarrow\uparrow\rangle\}$. The dimer excited states are a spin-1 triplet with quantum numbers $S^z = 1,0,-1$. To first approximation, the global ground state of the chain is a product of dimer singlets. However, the interdimer exchange (J') admixes a small amount (of the order $\sqrt{3}\alpha/8$) of polarized dimer pairs with total spin $s = 0$ as ground-state fluctuations [Fig. 1(e)]. The elementary excitations are a triplet of spin-1 states, or magnons. These are momentum k Bloch states obtained by exciting one dimer singlet to a triplet state. The interdimer coupling allows the excitation to hop from dimer to dimer along the chain, as illustrated in Fig. 1(f). To the lowest order in J', this one-magnon dispersion is $\omega(k) = J - (J'/2)\cos(kd)$.[16] The AHC then provides an excellent example of a one-dimensional system of hard-core quasiparticles if α is small.

Copper nitrate closely realizes the AHC, the Cu^{2+} ions have spin-1/2 moments, and the dominant exchange couplings are $J = 0.443 \pm 0.002$ meV and $\alpha = 0.227 \pm 0.005$. For these parameters, the magnon bandwidth is small compared to the gap. This parameter range is complementary to the one analyzed in recent studies.[4,6] Crucially the smallness of J'/J leads to a clear separation in energy between single-magnon excitations and two-magnon excitations, even at high temperatures. This allows for a detailed experimental investigation of the corresponding features in the dynamic response for a wide range of temperatures. Copper nitrate then is a particularly attractive material for studying the crossover in the dynamics between the low-temperature regime dominated by quantum fluctuations and the high-temperature phase characterized by thermal fluctuations.

Systems of one-dimensional hard-core bosons may also be realized as spin ladders, when the ratio of exchange parameters favors dimers forming on the rungs. Again, the hard-core constraint of magnons not being able to simultaneously occupy sites is enforced by the dimer units, which can only be in an unoccupied (singlet) or occupied state (one of the three triplet states). The thermal development of spectral weight in these ladder systems has been studied,[17,18] but the bond operator approaches used did not yield information about the linewidths, so that the results are somewhat complementary to those presented here.

The plan of the paper is as follows. In Sec. II, we outline the theoretical approach to calculating the finite-temperature response for the AHC. Section III covers the specifics of copper nitrate as a manifestation of the AHC. In Sec. IV, we compare the experimental results to the theoretical predictions. We also compare the data with exact diagonalization results in Sec. V. Finally, in Sec. VI, we make some concluding remarks.

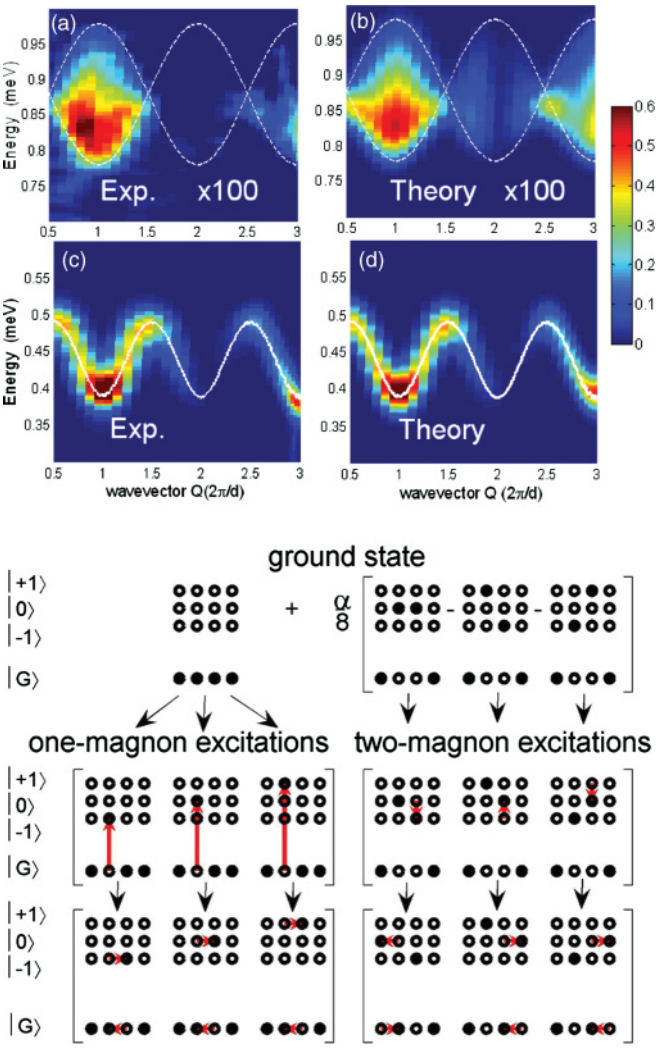

FIG. 1. (Color online) Excitation spectra of copper nitrate at $T = 0.12$ K (~0 K). (a) and (c) show background-subtracted two- and one-magnon experimental data, respectively, while (b) and (d) show the simulated $T = 0$ spectra. (e)–(g) presents schematically the excitation spectrum in terms of the single-dimer states. The ($|G\rangle, |+1\rangle, |0\rangle$, and $|-1\rangle$) open and filled circles represent unoccupied and occupied states. (e) represents the ground state where a small amount of the $s = 0$ two-magnon vacuum fluctuations mix with the dimer singlet. (f) shows the one-magnon excitation, where a singlet is promoted into a triplet and can then propagate along the chain, maintaining its polarization. (g) describes the two-magnon state where the $s = 0$ two-magnon fluctuations are excited; again these particles can propagate, maintaining polarization.

II. THEORY

An intrinsic property of the magnon excitations in the AHC is that they obey a hard-core constraint: each dimer site can be occupied by at most one magnon at a time. In addition to this hard-core repulsion, particles occupying neighboring

sites interact with each other through the interdimer exchange (J'). This interaction only exists for nearest neighbors and is absent for larger dimer separations. The nearest-neighbor potential V_s is $-J'/2, -J'/4, J'/4$ for pairs with combined total spin $s = 0,1,2$, respectively, and provides an attraction that has important effects on multiparticle states. There are two types of solutions to the two-particle Schrödinger equation:[19] The first has the form of a continuum of states, where k_1 and k_2 are momenta of the magnons along the chain, with total momentum along the chain $Q = k_1 + k_2$ and energy $\hbar\omega = \hbar\omega(k_1) + \hbar\omega(k_2)$. The scattering matrix (S matrix) describing the interchange of two particles in a state with total spin s is given by $S^s_{k1,k2}$, and the corresponding phase shift is $\phi^s_{k1,k2} = -(i/2)\ln(S^s_{k1,k2})$. We note that in general the S matrix differs from the noninteracting hard-core value $S^s_{k1,k2} = -1$, but reduces to the latter in the limit of vanishing momenta.

The second solution to the two-particle Schrödinger equation has the form of an exponentially decaying bound mode, which exists over all Q for $s = 0$ and around the nodes in the continuum ($Q \sim \pi/d$, where d is the chain repeat distance) for $s = 1$. For $s = 2$, the mode occurs at energies above the two-magnon continuum ("antibound mode").

A. Temperature

A fundamental result of this paper is the observation of the development of an asymmetric continuum with temperature. In general, the calculation of dynamical correlation functions at finite temperature is a highly nontrivial task. In Refs. 7 and 8 (and subsequently in Ref. 20), a method was developed and coupled with the property of integrability in certain one-dimensional systems to render the calculation tractable. However, the method can be applied without appealing to integrability if one is willing to work with approximate expressions for matrix elements (controlled by some small parameter, such as α). This has been done for both the AHC[9] and a dimerized spin ladder.[10] Other results for the dynamical correlations in the AHC at finite temperature have relied on exact diagonalization.[21] Here we calculate the spin response using the method described in Ref. 9, which is summarized below for convenience.

In the limit $\alpha = 0$ of decoupled dimers, the ground state for periodic boundary conditions is a product of local singlets,

$$|0\rangle = \prod_{j=1}^{N/2} |0\rangle_j = \prod_{j=1}^{N/2} \frac{1}{\sqrt{2}}[|\uparrow\rangle_{2j-1}|\downarrow\rangle_{2j} - |\downarrow\rangle_{2j-1}|\uparrow\rangle_{2j}]. \quad (1)$$

We have taken the stronger exchange J as between sites $j = 1,2$ and the weaker J' between $j = 2,3$, and so on for the rest of the chain. Single-particle excitations are obtained by exciting one dimer to a triplet state, e.g.,

$$t_0^+(m)|0\rangle_m = \frac{1}{\sqrt{2}}[|\uparrow\rangle_{2m-1}|\downarrow\rangle_{2m} + |\downarrow\rangle_{2m-1}|\uparrow\rangle_{2m}].$$

To the lowest order in degenerate perturbation theory, an excitation with $S^z = \sigma$ and momentum p is then given by (the repeat distance d is set to 2)

$$|p,\sigma\rangle = \sqrt{\frac{2}{N}} \sum_{m=1}^{N/2} e^{i2pm} t_\sigma^+(m)|0\rangle. \quad (2)$$

The energy of the one-particle states $|p,\alpha\rangle$ is

$$\epsilon(p) = J - \frac{J'}{2}\cos(2p). \quad (3)$$

By virtue of the periodic boundary conditions, the momenta take the values $p = 2\pi n/N$, $n = 0,1,\ldots N/2-1$. The leading-order expressions in degenerate perturbation theory for two-particle states with total spin s, z component of spin σ, and momenta $p_{1,2}$ are

$$|p_1,p_2,s,\sigma\rangle = N^s_{p1,p2} \sum_{m=2}^{N/2} \sum_{n=1}^{m-1} \psi_s(p_1,p_2|m,n) \times \sum_{\{\sigma_{1,2}\}} c^{s,\sigma}_{\sigma_1,\sigma_2} t^+_{\sigma_1}(m) t^+_{\sigma_2}(n)|0\rangle, \quad (4)$$

where $N^s_{p1,p2}$ is a normalization constant, $c^{s,\alpha}_{\sigma_1,\sigma_2}$ are Clebsch-Gordan coefficients, and the wave functions take the form

$$\psi_s(p_1,p_2|m,n) = e^{2i(p_1 m + p_2 n)} + S^s_{p1,p2} e^{2i(p_1 n + p_2 m)}. \quad (5)$$

The scattering matrix is given by

$$S^s_{p1,p2} = -\frac{1 + e^{-2i(p_1+p_2)} - 2\Delta_s e^{-2ip_2}}{1 + e^{-2i(p_1+p_2)} - 2\Delta_s e^{-2ip_1}}, \quad (6)$$

where $\Delta_0 = 1$, $\Delta_1 = 1/2$, and $\Delta_2 = -1/2$. Imposing periodic boundary conditions yields a set of coupled algebraic equations identical to the Bethe ansatz equations for the spin-1/2 Heisenberg XXZ chain with anisotropy Δ_s,

$$e^{ip_1 N} = S^s_{p1p2}, \quad e^{ip_2 N} = S^s_{p2p1}. \quad (7)$$

Explicit expressions for the wave functions are obtained by solving these equations numerically for the allowed values of $p_{1,2}$. Using these explicit forms of the wave functions, one can determine the matrix elements of the spin operators and, via a spectral representation, dynamical correlation functions. The dynamical susceptibility is given by

$$\chi^{zz}(\omega,Q) = -\int_0^\beta d\tau e^{i\omega_n \tau} \frac{1}{N} \times \sum_{l,l'} e^{-iQ(l-l')} \langle S^z_l(\tau) S^z_{l'} \rangle|_{\omega_n \to \delta - i\omega}, \quad (8)$$

where $\beta = 1/k_B T$. Using a spectral representation in imaginary time as well as translational invariance by two sites, we can express the susceptibility as

$$\chi^{zz}(\omega,Q) = \frac{1}{Z} \sum_{r,s=0}^{\infty} C_{rs},$$

$$C_{rs} = -\int_0^\beta d\tau e^{i\omega_n \tau} \frac{1}{N} \sum_{l,l'=0}^{N/2-1} e^{-2iQ(l-l')} \times \sum_{\gamma_r \gamma_s} e^{-\beta E_{\gamma_r}} e^{-\tau[E_{\gamma_s} - E_{\gamma_r}]} \times e^{i2(l-l')[P_{\gamma_s} - P_{\gamma_r}]} M_{\gamma_r \gamma_s}|_{\omega_n \to \delta - i\omega}. \quad (9)$$

Here, γ_s is a multi-index enumerating all s-particle states, E_{γ_s} and P_{γ_s} are, respectively, the energy and momentum of the

excited state $|\gamma_s\rangle$, and

$$M_{\gamma_r\gamma_s} = |\langle\gamma_r|S_0^z|\gamma_s\rangle|^2 + e^{iQ}\langle\gamma_r|S_0^z|\gamma_s\rangle\langle\gamma_s|S_1^z|\gamma_r\rangle + |\langle\gamma_r|S_1^z|\gamma_s\rangle|^2 + e^{-iQ}\langle\gamma_r|S_1^z|\gamma_s\rangle\langle\gamma_s|S_0^z|\gamma_r\rangle. \quad (10)$$

Carrying out the Fourier transform, we have

$$C_{rs} = \sum_{\gamma_r,\gamma_s} \frac{N}{4}\delta_{Q+P_{\gamma_r},P_{\gamma_s}} \frac{e^{-\beta E_{\gamma_r}} - e^{-\beta E_{\gamma_s}}}{\omega + i\delta + E_{\gamma_r} - E_{\gamma_s}} M_{\gamma_r\gamma_s}. \quad (11)$$

The terms C_{rs} in the expansion of the susceptibility contain contributions that diverge as system size to some power and are canceled by the partition function. In order to make these cancellations explicit, we denote the n-particle contribution to Z by Z_n and insert the expansion

$$Z^{-1} = \left(\sum_{n=0}^{\infty} Z_n\right)^{-1} = 1 - Z_1 - \left(Z_2 - Z_1^2\right) + \cdots \quad (12)$$

into the spectral representation of the susceptibility to obtain a low-temperature expansion of the form

$$\chi^{zz}(\omega,Q) = C_{01} + C_{10} + C_{11} + [C_{12} + C_{21} - Z_1(C_{01} + C_{10})] + \cdots \quad (13)$$

At $T > 0$, this expansion is found to exhibit divergences when $\omega \to \epsilon(Q)$ that grow with the number of particles. In order to obtain physically meaningful results, it is therefore necessary to carry out a resummation following Ref. 7. We first note that the result for the single-magnon contribution at $T = 0$ is obtained by taking into account only the ground state and one-particle states in the expansion of $\chi^{zz}(\omega,Q)$, resulting in

$$D(\omega,Q) = \frac{1-\cos(Q)}{4}\left[\frac{1}{\omega + i\delta - \epsilon(Q)} - \frac{1}{\omega + i\delta + \epsilon(Q)}\right]. \quad (14)$$

Casting the susceptibility at finite temperature in the form of a Dyson equation,

$$\chi^{zz}(\omega,Q) = \frac{D(\omega,Q)}{1 - D(\omega,Q)\Sigma(\omega,Q,T)}, \quad (15)$$

we obtain an expression $\chi^{zz} = [D(\omega,Q) + D^2(\omega,Q)\Sigma(\omega,Q,T) + \cdots]$ that exhibits the same type of divergences encountered in the spectral representation, which allows us to derive a low-temperature expansion for $\Sigma(\omega,Q,T)$ by matching the two expansions. To the leading order in $e^{-\beta J}$, we find

$$\Sigma(\omega,Q,T) \approx D^{-2}(\omega,Q)\{(C_{11} + C_{12} + C_{21}) - [Z_1(1 - e^{-\beta\epsilon(Q)}) + e^{-\beta\epsilon(Q)}]D(\omega,Q)\}. \quad (16)$$

The contributions C_{12}, C_{21}, and C_{11} are determined using the explicit forms of one- and two-magnon states given above and by solving the quantization conditions for magnon momenta numerically (which is easily done for systems of several thousand sites). This results in a low-temperature expansion of the dynamical susceptibility, controlled by the smallness of the density of thermally excited magnons. The derivation presented here is for a straight chain, but is easily adapted to more physically realistic systems.

III. COPPER NITRATE AND NEUTRON SCATTERING

A. Sample enrichment and growth

Due to the weak two-magnon scattering of about 1% of the one-magnon signal, a high-quality sample is crucial for a possible resolution of the two-magnon signal. In its original form, copper nitrate, $Cu(NO_3)_2{\cdot}2.5H_2O$, produces a high incoherent cross section due to the associated crystal water giving rise to an incoherent scattering signal. This can be avoided by replacing hydrogen with deuterium (D), which possesses a comparably low incoherent cross section (compare $\sigma_{\rm inc}H = 81b$ to $\sigma_{\rm inc}D = 2.03b$). This substitution is performed by several distillation runs.

The aim of the distillation process is the replacement of the crystal water associated with the copper nitrate powder by heavy water and the creation of a saturated solution. For the desired deuteration ratio of at least 98%, five distillation runs had to be implemented with the distillation process performed by using a rotary evaporator with its flask kept at 60 °C in a heat bath where the vacuum was never below 20 mbar so that the residual material kept its crystal solvate. The starting solution consists of a saturated heavy-water solution and additionally some extra heavy water for the pumping process and replacement of the crystal water, ensuring the existence of a solution during the whole distillation process.

For a saturated solution at 80 °C, the exact solubility of copper nitrate has to be established with the difficulty in determining the exact amount of crystal water H_2O enclosed in our starting material. Any contact with air below 26 °C will increase the crystal water in the material, changing the solubility, where the solubility is defined as the amount of $Cu(NO_3)_2$ dissolvable in a 100 g solution. Cost issues recommended the use of H_2O for the determination of the solubility for our starting material, and it was determined that 238.8 g of $Cu(NO_3)_2{\cdot}2.5H_2O$ could be dissolved in 50 g of H_2O at 80 °C, corresponding to a solubility of 66.7%, in good agreement with the tabulated value of 67.51%. This ratio has to be corrected due to the higher density of deuterium ($\rho_D = 1.107$ g/mol) compared to hydrogen. 238.8 g of the powder material $Cu(NO_3)_2{\cdot}2.5H_2O$ consist of 192.7 g of $Cu(NO_3)_2$ and 46.23 g of H_2O, resulting in a total of 96.23 g of H_2O for a saturated solution equivalent to 106.53 g of D_2O, establishing the total mass of a saturated heavy-water solution at 299.1 g.

The first distillation run is performed with recycled heavy water consisting of a deuteration ratio of at least 80% for which 262.4 g of D_2O are mixed to 238.8 g of $Cu(NO_3)_2{\cdot}2.5H_2O$, ensuring a deuteration mass ratio of at least 68.0% and an atomic ratio of 65.7%. During the distillation, 190.7 g of liquid are pumped out of the mixture, leaving 310 g of solution. The deuteration ratio does not change significantly during the distillation; if at all, a slight shift to a higher ratio is possible due to a 1.4 °C lower boiling point of H_2O compared to D_2O. For the second run, 253.4 g of D_2O are added to the remaining solution, raising the mass ratio to 89.9% and the atomic ratio to 88.8%; 263.3 g of liquid are pulled during the pumping process. The solution is replenished by 253.4 g of D_2O for the third run, creating a mass ratio of 96.9% (atomic ratio of 96.6%) and, during the distillation, 244.6 g of liquid are removed from the solution. In the second-to-last distillation

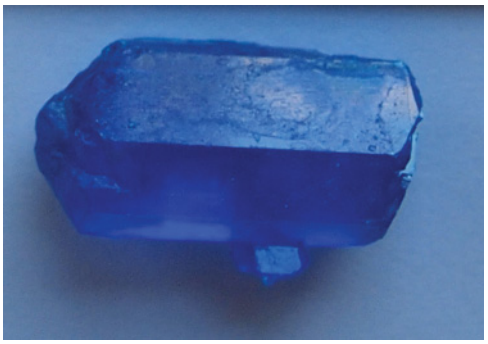

FIG. 2. (Color online) Example of a highly deuterated single crystal of copper nitrate grown using the solution growth and enrichment method described in Sec. III A of the text. Very large high-quality crystals of several tens of grams can be grown using this method.

run, a mass ratio of 99.0% and an atomic ratio of 98.9% are obtained by mixing 253.2 g of D_2O to the solution and, during the pumping, 259.6 g of liquid are extracted. For the last process, 230.0 g of D_2O are added and a mass ratio of 99.7% and an atomic ratio of 99.7% are reached. In this last distillation, 232.1 g of solution have to be extracted from the mixture to ensure a saturated solution for the growth process and, during the actual run, 233.7 g of liquid are pulled out. This amount is within the limits of having a saturated solution at 80 °C, leading to the decision to not add more D_2O in order to limit the air contact of the solution and thus a possible exchange between hydrogen and deuterium. By performing these five distillation runs, the target deuteration ratio of >99% is achieved.

This saturated solution in a sealed glass container is placed into a temperature-controlled oil bath at 85 °C. The liquid is cooled to 35 °C, well above the second phase-transition temperature, over several hours, producing needle-shaped seeds of approximate size 1 cm × 2 mm × 1 mm. Choosing one seed and placing the rest back into the solution to avoid any changes in the solubility, a thread is tied around the upper part of the seed and it is placed vertically into the solution. The thread has to be kept outside of the solution, ensuring the growth of the crystal below it and an easy removal after the completion of the growth process. The new starting temperature with the suspended seed consists of 65 °C to avoid any dissolving of the seed, and a cooling rate of 0.5 °C per hour until 45 °C is achieved, which is necessary for a homogeneous growth. The whole growth process is performed in a nitrogen-filled glove bag and resulted in the growth of the 8-g single crystal used in our neutron experiment. An example crystal grown using this method is shown in Fig. 2.

B. Neutron scattering

The single and multiparticle states were measured using the OSIRIS indirect geometry time-of-flight spectrometer[22] at the ISIS Facility, Rutherford Appleton Laboratory, United Kingdom. The crystal was precisely aligned with the $(h,0,l)$ reciprocal lattice plane in the horizontal scattering plane. $Cu(NO_3)_2{\cdot}2.5(D_2O)$ is monoclinic ($I12/c1$) with lattice parameters (at 3 K) of $a = 16.1$, $b = 4.9$, and $c = 15.8$ Å and $\beta = 92.9°$.[23] Equivalent chains lie along the [1,1,1]/2 and [1,−1,1]/2 directions and project onto the same direction on the $(h,0,l)$ plane.[19] A dilution insert provided sample temperatures down to 120 mK and a rotation stage allowed the magnetic chains to be rotated to different angles relative to the incident beam of neutrons. A white beam is pulsed at 50 Hz with neutrons arriving at the sample over the initial 34-m flight path at different times according to their energy. An array of pyrolytic graphite analyzers scatter neutrons with energy of 1.845 meV from 002 reflections into a bank of 42 detectors, covering scattering angles from 11° to 150° arrayed at 0.5 m around the sample, provided an energy resolution of 25 μeV full width at half maximum. The cooling of the analyzers in OSIRIS provides a very low background by removing thermal diffuse scattering. The energy and wave-vector transfer of scattering events are calculated from the crystal angle and converted to the partial differential cross section expressed in terms of the projection of the wave vector along the chain axis. Nonmagnetic backgrounds have been subtracted from the displayed data sets.

At very low temperatures compared to the exchange energy J, neutrons essentially measure the $S = 1$ spectrum by exciting from the ground state. The entire scattering plane was measured and the single-magnon excitation spectrum was fitted to determine the exchange couplings using a simple cosinusoidal dispersion, $\hbar\omega(\mathbf{Q}) = J - 1/2 \sum_{\mathbf{d}} J_{\mathbf{d}} \cos(\mathbf{Q}\cdot\mathbf{d})$. This analysis showed that the strongest exchange, $J = 0.443 \pm 0.002$ meV, is across the bond [0.234, ±0.473, 0.270] with intradimer $J_{[0.266,0.027,0.230]} = 0.101$ meV, giving the alternation ratio $\alpha = J/J = 0.227 \pm 0.005$. The interchain coupling along the [1/2,0,0] and [0,0,1/2] directions are $J_a = 0.006 \pm 0.003$ meV and $J_c = 0.0018 \pm 0.0005$ meV. The improved exchange-parameters determination was possible due to the comprehensive and high-quality data sets obtained from OSIRIS.

IV. RESULTS AND DISCUSSION

A. One-magnon, two-magnon, and bound states

In Fig. 1, the excitations to the one-magnon modes are easily seen and follow accurately the predicted cosinusoidal behavior. The wave-vector modulation of the intensity is due to interference in scattering between the two spins composing the dimer. The two-quasiparticle states can also be observed. Neutrons scatter from the weakly admixed polarized ($s = 0$) dimer pairs composing the ground-state fluctuations to the two-magnon states [Fig. 1(g)]. This scattering is far more sensitive to the composition, interactions, and phase factors between particles than the one-magnon signal, and our measurements, given in Fig. 3, are in quantitative agreement with the interacting two-particle Schrödinger wave functions, calculated in the appendix of Ref. 19. In particular, we resolve the spin-1 bound mode of the AHC, which is a direct signature of the two-particle interaction, given in Figs. 3(c) and 4. The binding energy and intensity of the bound mode are in perfect agreement with the perturbative calculation.[13] This confirms that copper nitrate accurately realizes an interacting gas of hard-core magnons in one dimension and shows an attractive

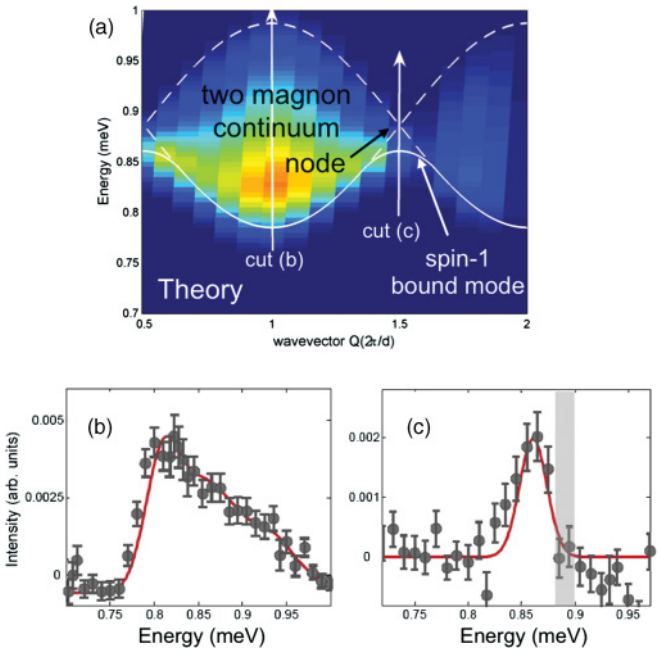

FIG. 3. (Color online) The two-magnon states. (a) The superimposed line gives the upper and lower boundaries of the two-magnon scattering and the position of the bound mode, lying just below the node. (b) is a cut of the scattering intensity at $Q = 2\pi/d$ as a function of energy; scattering is observed between the upper and lower two-magnon envelope. (c) is a cut at the node position ($Q = 3\pi/d$). The node occurs at an energy of 0.88 meV (shaded region), however, at this wave vector, it is predicted to have very little intensity. Red lines are calculations based on the two-particle Schrodinger solution.[19] A peak is nevertheless observed and occurs at the lower energy of 0.855 meV; this is the expected position of the bound mode.

coupling—the bound state appears below the continuum—between pairs of magnons in a spin-1 total state. Magnons in the spin-0 total state are even more attractive and form a deeper bound state not visible to neutrons, while the magnons are repulsive in spin-2 states and form an antibound state above the continuum, again not visible to neutron scattering due to spin conservation selection rules.

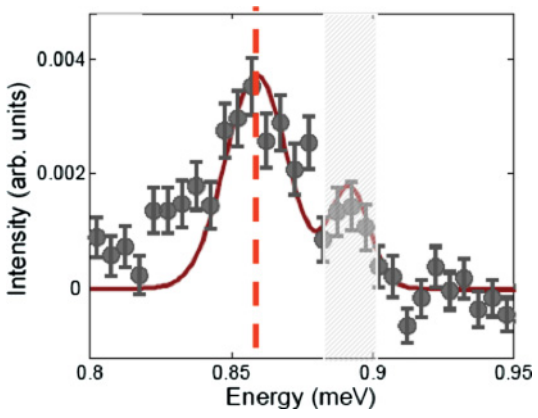

FIG. 4. (Color online) Measurement showing bound mode at ∼0.86 meV, as indicated by the red dashed line, resolved from the continuum at the higher energy of ∼0.89 meV, with gray hatching indicating the nominal extent of the continuum. The measurement here was made with a different crystal rotation angle from that in Fig. 3(c) and cuts through a location with more intensity near the continuum node. The red line is that of two resolution-broadened Gaussians at the expected bound mode and continuum positions.

The spin-1 bound mode, shown in Fig. 3(c), is extracted from a crystal orientation that covers the whole wave-vector extent of the continuum. In this geometry, the node in the continuum has very little intensity and only the bound mode is apparent. Other crystal rotations, while not covering the whole wave-vector range simultaneously, can provide the possibility to observe bound mode and continuum scattering simultaneously, as shown in Fig. 4.

B. Thermal effects

At low temperatures, the dynamics of the strongly alternating Heisenberg chain can be thought of in terms of a low-density gas of hard-core magnons. We follow the thermal evolution of correlations in this quasiparticle gas: The density of thermally excited magnons per dimer can be estimated from the zero-bandwidth limit to be $n(T) \approx 3\exp(-J/kT)/[1 + 3\exp(-J/kT)]$ (black dash-dotted line in Fig. 5). Neutron-scattering measurements were made at temperatures of $T = 0.12,2,3,4,6$ K, where the magnon densities are approximately $n = 6 \times 10^{-19}$, 0.19, 0.35, 0.45, 0.56, respectively, and where the density at infinite temperature is $n(\infty) = 0.75$. With increasing temperature, the following picture emerges: first, the two-magnon scattering all but disappears; second, a new band of scattering emerges around zero energy with the same bandwidth as the one-magnon scattering; and third, the one-magnon mode develops into a scattering continuum; see Fig. 6.

The decrease in the two-particle scattering with increasing temperature is a direct result of the hard-core constraint. A neutron cannot create a further two magnons on a given pair of

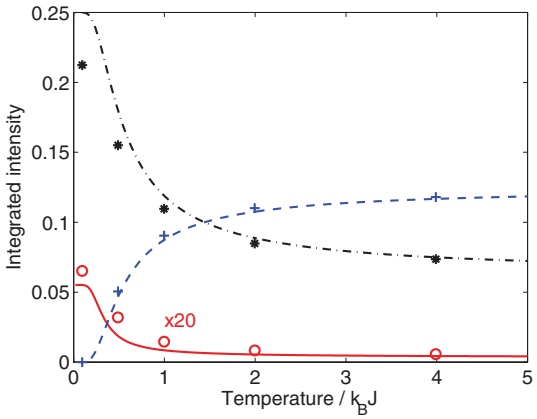

FIG. 5. (Color online) Calculated integrated intensity of the one-magnon band (black stars), two-magnon band (red circles; note the intensity is scaled by a factor of 20 to be visible on the same scale), and central quasielastic band (blue crosses), as computed in Ref. 21 using 16 spin diagonalizations for copper nitrate. The temperature is rescaled to the dimer energy J. The black dash-dotted line is the zero bandwidth limit result discussed in Sec. IV B, and the blue dashed line is the corresponding value for the central peak (see Ref. 7). The red solid line is the intensity predicted for the two-magnon scattering from perturbation theory; see Sec. IV B.

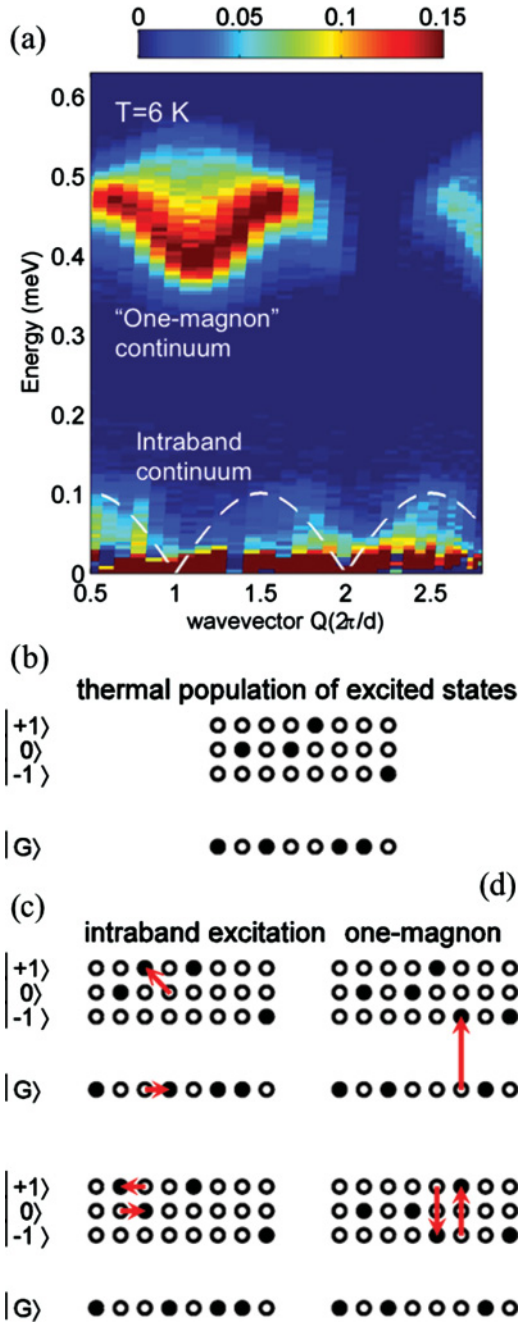

FIG. 6. (Color online) Excitations at finite temperature. (a) shows the experimental data at 6 K. The one-magnon scattering has significant asymmetric broadening at this temperature; additional scattering appears around $E = 0$ meV. This is intraband scattering, which at the lowest temperatures is found only within the white boundary shown. (b)–(d) gives a schematic representation of the neutron-scattering processes. At finite temperature, a significant number of dimer triplets are thermally excited, as shown in (b). Neutrons can scatter these magnons within the triplet band, which is observed as the intraband scattering. (c) One-magnon excitations can also be made by exciting a dimer from a singlet to a triplet as before. (d) However, now in addition to the energy gap, the interaction of the magnons within the band must be considered, as must the hard-core constraint; these effects combine to give an asymmetric line shape as described in the text.

dimers if any of the dimers is already occupied by a magnon. The density of adjacent dimer pairs that are both unoccupied falls approximately as $n_{ss}(T) \approx 1/[1 + 6\exp(-J/kT) + 9\exp(-2J/kT)]$, i.e., $n_{ss} = 1, 0.66, 0.42, 0.30, 0.19$, respectively, for temperatures 0.12, 2, 3, 4, 6 K, and reaches a value of $n_{ss}(\infty) = 0.0625$ at infinite temperature. The expected intensity is a product of the matrix element $\alpha^2/4$ (to lowest order in α) and the population of unoccupied pairs, and therefore is proportional to $I_{2\text{magnon}} \approx n_{ss} \times \alpha^2/4$ (see Fig. 5 where this result, shown as a red solid line, is compared to exact diagonalization). This implies that the two-magnon band does not disappear altogether, but rather becomes very hard to detect, with an intensity of only 0.06% of the total scattering at high temperature.

C. Intraband scattering

Around zero energy, a central peak in $S(Q,\omega)$ appears with increasing temperature due to intraband scattering within the one-magnon band: Neutrons can scatter via a change in momentum and energy (and possibly spin quantum number) off of a thermally excited magnon, as shown in Fig. 6. Precisely one scattering process exists for given wave vector Q and frequency ω in a frequency range $|\omega| < \omega_m(Q)$ [where the maximum frequency $\omega_m(Q = \pi)$ is the bandwidth]. To the lowest order, we have $\omega_m(Q) = \alpha J \sin(Q/2)$, and from the density of states a square root at $\pm\omega_m(Q)$ results. In the higher order, this singularity becomes rounded out to a continuum.[9] Results for the line shape of the central peak are displayed in Fig. 7(c). The calculated intraband scattering for $Q = \pi$ for different temperatures are also shown in Fig. 7(c). Although the central regime at energy zero is masked by other incoherent scattering processes from the material, the increase of signal toward ω_m and the drastic decrease beyond ω_m is clearly seen.

The basic square-root singularity characterizing this scattering process appears similar to the scattering from excited domain walls in quantum Heisenberg-Ising chains, as predicted by Villain[24] and observed later in the quasi-1D magnets, $CsCoCl_3$ (Refs. 25 and 26) and $CsCoBr_3$ (Ref. 27). However, this similarity is to a large extent formal (cosine spectrum of the basic excitation), whereas the basic processes behind the scattering are very different:[9,28] In the AHC, the leading contribution to the intraband scattering at low temperatures arises from scattering processes between two well-defined single-particle states. On the other hand, spin excitations in the Heisenberg-Ising chain occur in pairs of domain walls and the leading contribution to the low-temperature intraband scattering is due to scattering on one member of the domain-wall pair. While the topological nature of these solitonlike excitations restricts it to 1D, the dimer case studied here can serve as a paradigm for gapped quantum magnets in any number of dimensions. In particular, intraband scattering is also present in other gapped quantum spin chains such as Haldane-gap compounds, but is likely to be more spread out and harder to observe due to the larger ratio of bandwidth to gap energy.

D. Thermal line broadening

Finally, we discuss the asymmetrically broadened line shape of the one-magnon scattering at finite temperature. In a

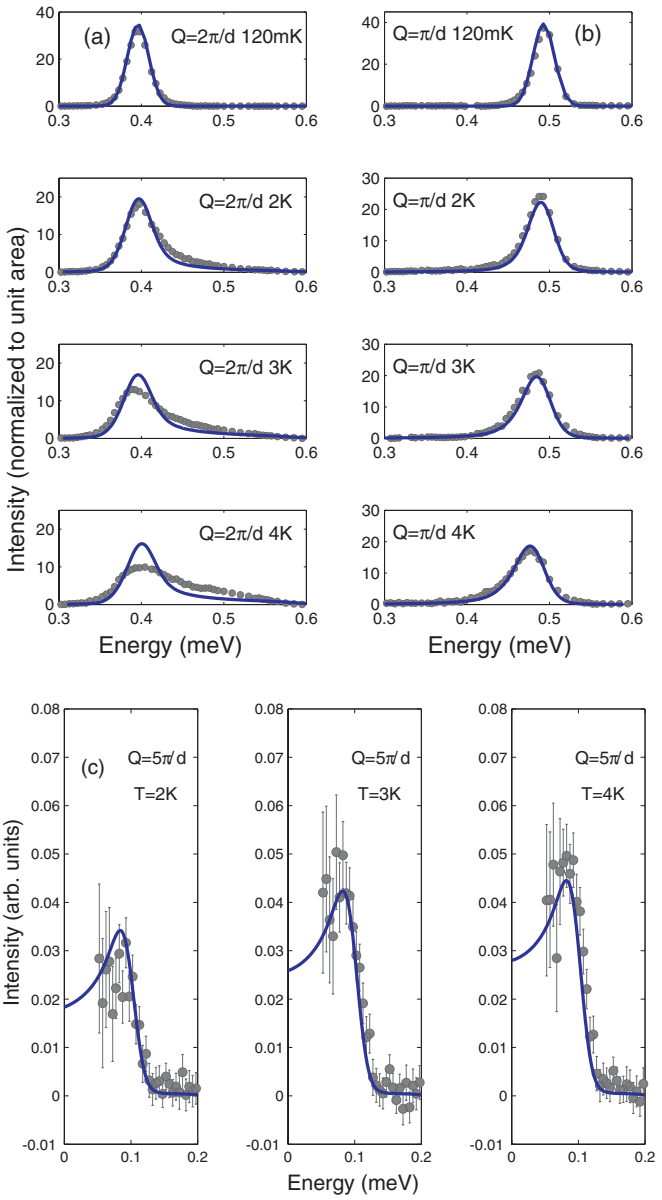

FIG. 7. (Color online) Temperature dependence of intraband and one-magnon excitations: (a) shows the one-magnon scattering for $Q = 2\pi/d$ at 2, 3, and 4 K, respectively. (b) shows the one-magnon at $Q = \pi/d$ for 2, 3, and 4 K. The profile becomes broadened with temperature and develops an asymmetric line shape. (c) shows the intraband scattering at $Q = 5\pi/d$; the scattering is similar at π/d and $3\pi/d$ but the background is particularly clean at $Q = 5\pi/d$. A theory of interacting particles was developed as described in Sec. II and is shown as the solid blue line in each panel of parts (a)–(c) (convolved with the experimental resolution). Note that for 4 K, the agreement is not as good because the series expansion is only valid at low particle density.

semiclassical picture, the high-temperature or paramagnetic phase is characterized by an absence of coherence, and quasiparticles only emerge with decreasing temperature. The process can be followed in the one-particle scattering, where the neutron creates a magnon directly by polarizing an unoccupied dimer. In such a picture, a symmetric Lorentzian line shape is predicted, whose width is a measure of the lifetime or coherence of the particles. The issue was first addressed experimentally by Xu *et al.*[23] who also studied one-magnon scattering in copper nitrate using inelastic neutron scattering (INS). The data was interpreted as a conventional Lorentzian line shape and modeled using a random phase approximation (RPA) calculation. The dispersion of these particles was found to renormalize with temperature with the bandwidth of the excitation spectrum narrowing compared to an RPA calculation. Here we find that the lineshapes are in fact highly asymmetric in energy. This suggests that a Lorentzian broadening occurs only at very low temperatures (compared to the magnon gap), which is a fact that is borne out by calculations above in Sec. II. At higher T, magnon interaction effects are such that a simple description in terms of a lifetime no longer applies. The line shape then constitutes a fingerprint of the magnon interactions.

Figure 7 shows the thermal evolution of the one-magnon band. The most striking feature is the formation with increasing temperature of a continuum of scattering weighted toward higher (lower) energies for $Q = 2\pi/d$ ($Q = \pi/d$ and $Q = 3\pi/d$). In the analysis of experimentally obtained lineshapes that show asymmetric thermal broadening, such as those presented here, it is useful to have a function that can be fit to the data, parametrizing the asymmetry. We find a suitable function to be

$$I(Q,\omega) = A(Q)\int_{-\infty}^{\infty} dt \frac{\exp\left\{-\frac{[\omega-\Gamma(Q)t-d(Q)]^2}{2\sigma^2}\right\}}{\sqrt{2\pi\sigma^2}} \times \frac{1}{\pi}\frac{1}{1+\left(t-\alpha(Q)t^2+\gamma(Q)t^3\right)^2}. \quad (17)$$

This incorporates the effect of the experimental resolution by taking a convolution with a Gaussian of variance σ (we have made a substitution, shifting and rescaling the integration dummy parameter to simplify the integrand). The remaining function takes the form of a modified Lorentzian, where the usual argument has been replaced by a polynomial that includes an asymmetry term, $\alpha(Q)t^2$, and a further damping term, $\gamma(Q)t^3$. As $T \to 0$, the asymmetry vanishes $[\alpha(Q),\gamma(Q) \to 0]$ and the line shape becomes Lorentzian (broadened by the experimental resolution). Taking the $T = 0.12$ K data as symmetric, we extract the resolution, $\sigma = 0.12$ meV, and use this as an input parameter for fits at $T = 2,3,4$, and 6 K. The extracted parameters are then $\Gamma(Q)$, $d(Q)$, $\alpha(Q)$, $\gamma(Q)$, and the overall amplitude $A(Q)$. Some of the fits obtained are shown in Fig. 8. A simple measure of the asymmetry is given by $\alpha(Q)$, which is increasingly positive (negative) for a tail weighted toward higher (lower) energies. In Fig. 9, we plot the values of $\alpha(Q)$ and $\Gamma(Q)$ obtained using Eq. (17).

E. Interacting particle gas

To gain insight into the development of the asymmetric line shape, a calculation was presented in Sec. II, treating the thermally excited particles as a strongly correlated quantum ensemble. These calculated lineshapes (blue line) for the alternating Heisenberg chain at finite temperature are also shown in Fig. 7 and give a good account of the data.

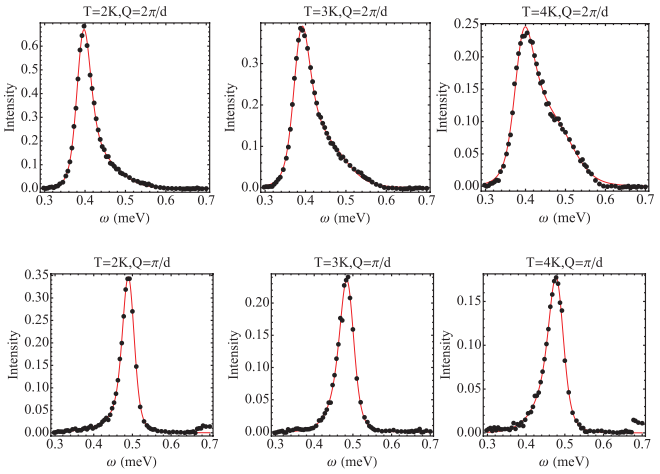

FIG. 8. (Color online) Fits (red curves) of Eq. (17) to the experimental data (black points). Parameters are obtained by first fitting a Lorentzian convolved with a Gaussian to the $T = 120$ mK data in order to extract the experimental resolution.

For hard-core particles with no contact potential, the quasiparticles are fermionic in the sense that their scattering matrix is -1. They are hard core in that even if the fermions have different spin quantum numbers, they will never occupy the same dimer site. The broadening of the magnon line is found to be highly asymmetric in this case. The presence of a further interaction in the form of a contact potential ("stickiness") between quasiparticles is seen to modify the line shape. This demonstrates that as expected on general grounds, the broadening of the line reflects the details of the quasiparticle interactions. On a qualitative level, the broadening of the magnon line can be understood by considering the joint density of states for transitions between thermally occupied one-magnon states and unoccupied two-magnon states,

$$N_{1\to 2} = \sum_{p,p_1,p_2} n(p)\bar{n}(p_1,p_2)\delta_{q+p,p_1+p_2}\delta_{\omega+\omega(p),\omega(p_1)+\omega(p_2)}. \tag{18}$$

Here, $n(p)$ is the thermal occupation number for a one-magnon state with momentum p and $\bar{n}(p_1,p_2)$ is the probability that the two-magnon state characterized by momenta p_1, p_2 is unoccupied. For $-\pi/2d < Q < \pi/2d$ and $\pi/2d < Q < 3\pi/2d$, this function is skewed toward higher and lower energies, respectively. The specific form of the line shape is dictated by the matrix element and hence by the magnon-magnon interaction.

Again, one may naïvely think that formation of the one-magnon band as a continuum resembles the two-soliton continua in the quantum Heisenberg-Ising chains, such as $CsCoCl_3$ (Refs. 25 and 26) and $CsCoBr_3$ (Ref. 27). However, this is misleading. The physical origin is distinctly different with the continuum in the quantum Heisenberg-Ising chains due to the neutron-scattering process involving a spin-1 flip being projected into pair states consisting of two solitons each, carrying a spin-1/2 and independent momenta and energy. The partitioning of momenta and energy is a simple summation, $E = E(k_1) + E(k_2)$ and $k = k_1 + k_2$, which gives a characteristic bowtie structure, and this continuum is a $T = 0$ property of the Hilbert space. For the AHC, the excitations are spin-1 magnons with only one being excited by a neutron. There is no one-magnon continuum at $T = 0$, only a δ-function pole. At elevated temperatures, the neutron-excited magnon interacts with the nearby thermally activated magnons through the potential V and scatters to a two-magnon final state via an off-shell scattering process. The continuum in Eq. (18) then is distinctly different in extent in wave vector and energy.

This behavior then represents a quite different paradigm for the effects of temperature in a quantum magnet, in contrast to the expectation of simple lifetime broadening due to thermal decoherence that is observed, for example, in the 2D Heisenberg antiferromagnet.[3] We expect that such strongly correlated physics is generic to ensembles of interacting hard-core particles and should be seen mainly in low-dimensional gases of particles including other gapped quantum magnets.

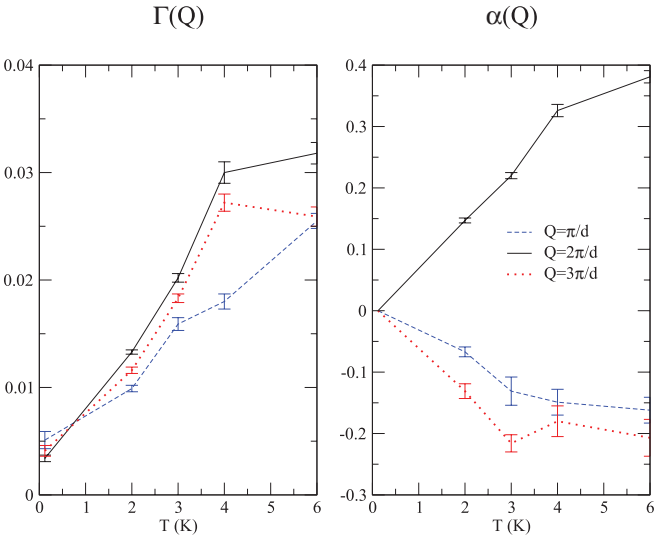

FIG. 9. (Color online) The Lorentzian width $\Gamma(Q)$ and asymmetry $\alpha(Q)$ extracted from fits of Eq. (17) to the experimental data at 0.12, 2, 3, 4, and 6 K. Fits are obtained by first fitting a Lorentzian convolved with a Gaussian to the $T = 120$ mK data in order to extract the experimental resolution.

V. COMPARISON TO DIAGONALIZATIONS

Complementing the above analytical approach, an exact finite chain diagonalization study using 16 sites has been undertaken for the spin-1/2 alternating Heisenberg chain with the parameters for copper nitrate.[21] The scattering, including all possible transitions, weighted by thermal population and scattering cross sections and corrected for both the magnetic form factor for Cu^{2+} and the instrumental resolution, has been computed. These computations also predict the asymmetric line shape in agreement with the measurements, demonstrating an accurate handling of background effects in the neutron-scattering data. The temperature dependence of the one-magnon lineshapes, both measured and computed, are shown in Fig. 10, which demonstrates very good agreement. The small disagreement at 2 K is probably due to the sample being at a slightly elevated temperature during the measurement. The

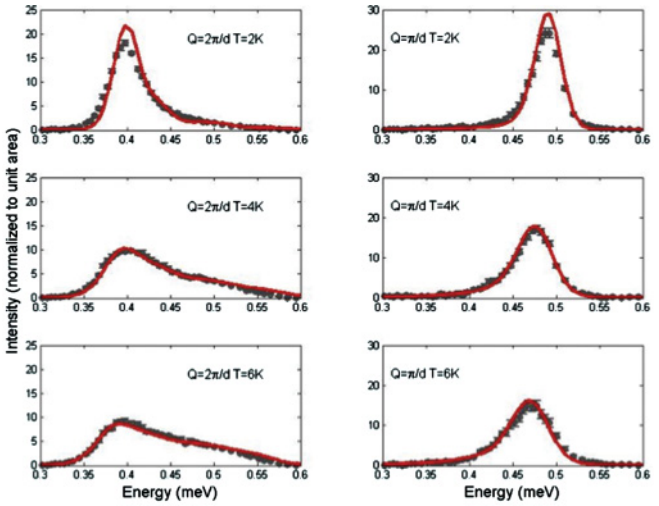

FIG. 10. (Color online) The one-magnon line shape at different temperature (2, 4, 6 K) compared to the exact diagonalization calculations for $Q = 2\pi/d$ (left-hand panels) and $Q = \pi/d$ (right-hand panels). Small corrections for interchain coupling have been made to the lineshapes generated assuming $J = 0.443$ meV and $J'/J = 0.226$. Also, the intensity is normalized to unit area to simplify the prefactor contributions of thermal weight and dimer structure factor.

intraband scattering is centered on zero energy transfer. This is particularly hard to measure because the incoherent scattering of hydrogen from the sample gives a large background signal centered at 0 meV. The excellent energy resolution of OSIRIS allows the magnetic intraband signal to be extracted at around twice the FWHM of the energy resolution. In fact, reliable data is extracted from 0.048 meV transfer and above. The accurate handling of background effects in the neutron-scattering data is again demonstrated by the comparison with the computed lineshapes. The temperature dependence of the intraband scattering agrees very well in intensity, and line shape changes with the computations, as shown in Fig. 11.

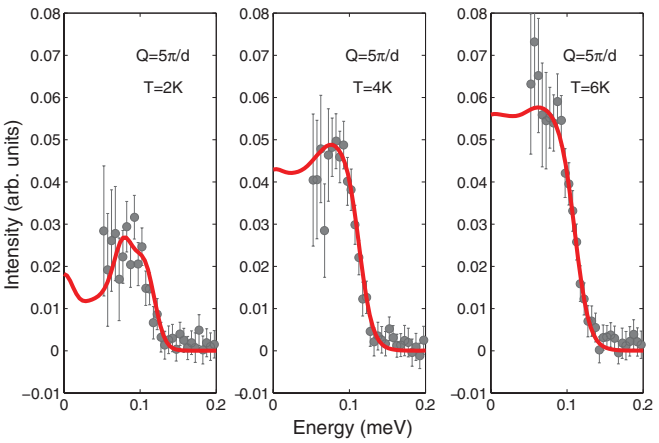

FIG. 11. (Color online) The intraband scattering at different temperatures (2, 4, 6 K) compared to the exact diagonalization calculations. At 2 K, the vestiges of the singularity at the upper boundary (Villain-type mode) are seen. The agreement with the finite chain calculations[21] including instrumental resolution is excellent.

Finally, we draw attention to Fig. 3 from Ref. 21, which shows $S(Q,\omega)$ calculated via the 16 spin diagonalization. It shows a cut at π/d, and at $2\pi/d$ with no instrumental resolution (cf. Fig. 8 in this paper). For both π/d and $2\pi/d$, the asymmetry of the line shape is very clearly seen at the different temperatures. Note that the copper nitrate parameters were used, and the temperature and energy scales are in units of the dimer coupling, $J = 0.443 \pm 0.002$ meV. This shows that the line asymmetry indeed survives up to all orders of perturbation (i.e., to temperatures of the order of the gap and above) and is a striking physical effect.

VI. SUMMARY AND CONCLUSION

We have undertaken an in-depth study of the effects of temperature on a gapped quantum magnet. By using inelastic neutron scattering, the dynamics in the model one-dimensional magnet, copper nitrate, was determined at a series of temperatures. The primary observations are (1) a thermally induced central peak due to intraband scattering, and (2) the one-magnon quasiparticle pole is seen to develop with temperature into an asymmetric continuum of scattering, rather than showing the conventional Lorentzian line broadening. To complement the experimental measurements, theoretical calculations and finite chain diagonalizations specialized to the spin-1/2 one-dimensional (1D) bond alternating Heisenberg chain describing copper nitrate are combined to interpret the physical origin of the thermal effects observed. The central peak is shown to have a physical origin similar to Villain scattering familiar from soliton systems in 1D. However, here the excitations are boson quasiparticles, which do not have the same dimensional constraints of topological solitons and so generalize to dimensions greater than one and this should be searched for in other materials. As regards the one-particle band, we relate this asymmetric line broadening to hard-core constraints and quasiparticle interactions, and this can be explained as a scattering process whereby a quasiparticle is inserted into a partially filled multiparticle band. The asymmetry originates from a combination of the density of states of the transitions available and the interaction potential modifying the cross section. These findings are a counter example to recent assertions of the universality of line broadening in 1D systems, which assume a Lorentzian line broadening. Indeed, the computations show asymmetry relevant at even the lowest temperatures. The results are applicable to a broad range of quantum systems.

In conclusion, our study shows that the effects of temperature in a low-dimensional quantum magnet are not those of simple decoherence of the quasiparticles, but instead promote the formation of a strongly correlated gas of quasiparticles. A description of this state has been achieved using non-perturbative methods. The findings here should apply to a large range of quantum systems and present a model of such behavior.

ACKNOWLEDGMENTS

We thank Rick Paul (NIST) for measuring the deuteration of the sample, S. Pfannenstiel (HZB) for storage, Felix Groitl

(HZB) for photograghy, and K. Damle (TFIR Mumbai) for enlightening discussions. Work at the Ames Laboratory was supported by the US Department of Energy, Basic Energy Sciences, under Contract No. DE-AC02-07CH11358.

[1] S. P. Bayrakci, T. Keller, K. Habicht, and B. Keimer, Science **312**, 1926 (2006).
[2] H. M. Ronnow, D. F. McMorrow, R. Coldea, A. Harrison, I. D. Youngson, T. G. Perring, G. Aeppli, O. Syljuasen, K. Lefmann, and C. Rischel, Phys. Rev. Lett. **87**, 037202 (2001).
[3] T. Huberman, D. A. Tennant, R. A. Cowley, R. Coldea, and C. D. Frost, J. Stat. Mech. (2008) P05017.
[4] G. Y. Xu *et al.*, Science **317**, 1049 (2007).
[5] S. Sachdev, *Quantum Phase Transitions* (Cambridge University Press, Cambridge, 1999).
[6] A. Zheludev, V. O. Garlea, L. P. Regnault, H. Manaka, A. Tsvelik, and J. H. Chung, Phys. Rev. Lett. **100**, 157204 (2008); M. Kenzelmann, R. A. Cowley, W. J. L. Buyers, and D. F. McMorrow, Phys. Rev. B **63**, 134417 (2001).
[7] F. H. L. Essler and R. M. Konik, Phys. Rev. B **78**, 100403 (2008).
[8] F. H. L. Essler and R. M. Konik, J. Stat. Mech. (2009) P09018.
[9] A. J. A. James, F. H. L. Essler, and R. M. Konik, Phys. Rev. B **78**, 094411 (2008).
[10] W. D. Goetze, U. Karahasanovic, and F. H. L. Essler, Phys. Rev. B **82**, 104417 (2010).
[11] G. S. Uhrig and H. J. Schulz, Phys. Rev. B **54**, R9624 (1996).
[12] C. J. Hamer, W. Zheng, and R. R. P. Singh, Phys. Rev. B **68**, 214408 (2003).
[13] K. P. Schmidt, C. Knetter, and G. S. Uhrig, Phys. Rev. B **69**, 104417 (2004).
[14] C. Brukner, V. Vedral, and A. Zeilinger, Phys. Rev. A **73**, 012110 (2006).
[15] V. Srinivasa, J. Levy, and C. S. Hellberg, Phys. Rev. B **76**, 094411 (2007).
[16] T. Barnes, J. Riera, and D. A. Tennant, Phys. Rev. B **59**, 11384 (1999).
[17] I. Exius, K. P. Schmidt, B. Lake, D. A. Tennant, and G. S. Uhrig, Phys. Rev. B **82**, 214410 (2010).
[18] B. Normand and Ch. Rüegg, Phys. Rev. B **83**, 054415 (2011).
[19] D. A. Tennant, C. Broholm, D. H. Reich, S. E. Nagler, G. E. Granroth, T. Barnes, K. Damle, G. Xu, Y. Chen, and B. C. Sales, Phys. Rev. B **67**, 054414 (2003).
[20] B. Pozsgay and G. Takács, Nucl. Phys. B **788**, 209 (2008); J. Stat. Mech. (2010) P11012.
[21] H.-J. Mikeska and C. Luckmann, Phys. Rev. B **73**, 184426 (2006).
[22] M. T. F. Telling and K. H. Andersen, PhysChemChemPhys **7**, 1255 (2005).
[23] G. Y. Xu, C. Broholm, D. H. Reich, and M. A. Adams, Phys. Rev. Lett. **84**, 4465 (2000).
[24] J. Villain, Physica B **79**, 1 (1975).
[25] J. P. Boucher, L. P. Regnault, J. Rossat-Mignod, Y. Henry, J. Bouillot, and W. G. Stirling, Phys. Rev. B **31**, 3015 (1985).
[26] H. B. Braun *et al.*, Nature Phys. **1**, 159 (2005).
[27] S. E. Nagler, W. J. L. Buyers, R. L. Armstrong, and B. Briat, Phys. Rev. Lett. **49**, 590 (1982).
[28] A. J. A. James, W. D. Goetze, and F. H. L. Essler, Phys. Rev. B **79**, 214408 (2009).